İSTANBUL UNIVERSITY CERRAHPAŞA

ORIGINAL ARTICLE
Electrica 2023; 23(1): 87-94

Vector-Controlled Permanent Magnet Synchronous Motor Drive with Reduced Current Sensor

Sai Shiva Badini, Vimlesh Verma

Department of Electrical Engineering, National Institute of Technology Patna, Patna, India

Cite this article as: S. Shiva Badini and V. Verma, "Vector-controlled permanent magnet synchronous motor drive with reduced current sensor," *Electrica*, 23(1), 87-94, 2023.

ABSTRACT

This study presents an algorithm for estimating two-phase rotor reference frame currents using a single-current sensor. For proper vector control operation, at least two of three-phase current information is required. The single-current sensor algorithm is presented for vector-controlled interior permanent magnet synchronous motor drive to reduce the cost and increase reliability. dq-axes current formation method evaluates the two-phase currents in the stationary reference frame by sensing only one-phase current and speed/position information. The two-phase stationary reference frame currents, $i_{\beta s}$ current, are estimated using i_{qs}^{*} and $i_{\alpha s}$, i.e., constructed from single sensor information. *D*- and *q-axes* currents are obtained from $i_{\alpha s}$ and $i_{\beta s}^{*}$. These are used to close the current loop in the vector-controlled drive. Three-phase currents can be reconstructed from the estimated two-phase currents. This method is entirely independent of machine parameters and applicable to all kinds of permanent magnet synchronous motor machines. The presented algorithm is validated on MATLAB/SIMULINK platform. Some sample results are shown from an experiment performed on a prototype developed in the laboratory (using dSPACE 1104).

***Index Terms*—**Current estimation, dSPACE, IPMSM, single-current sensor, vector control

I. INTRODUCTION

The trend toward electric vehicles is rapidly increasing in recent years. Current, permanent magnet synchronous motor (PMSM) is receiving much attention for electric drive operation with its capability of propelling at different speeds, higher torque to inertia, high efficiency, simple controlling structure, compact in size, and high power density [1]. Vector-controlled drive is widely used in industrial applications because of its superior dynamic performance [2]. Position/speed information is procured from the shaft encoder, which is essential to close the outer loop (i.e., speed loop), and position information is used in voltage and current coordinate transform in the vector-controlled drive. The reliability and monitoring of drive rely on knowing mechanical and electrical variables such as speed/position and current.

In general, a PMSM drive requires at least two current sensors and one speed/position sensor [1-3]. Mounting a sensor to a machine will increase the drive's size and cost, and any disturbance in the sensor will deteriorate the performance. Elimination of the speed sensor/encoder will make the system more robust, and drive will be relatively cheaper. Many solutions are available in the literature for the drive speed sensorless operation [1, 4-13].

The effects of current measurement errors including offset error and scaling error will affect the drive [14]. The sudden failure of any current sensors leads to heavy current flow. It affects both machine and inverter circuitry. These [15-18] methods are used alternately to measure and monitor the complete drive to avoid such conditions. This study is mainly concerned on reducing the drive reliability on current sensors and increasing safety. There are some single current sensor methods presented in the literature [14-20]. Phase currents are obtained directly or indirectly by using a single current sensor. The single-current sensor approach is presented in [15, 21-27]; here, three-phase currents are constructed based on the DC-link current and switching information of the inverter. It is a conventional approach with the following limitations: (i) under-low modulation index, (ii) near to sector boundary/short duration of the active-switching states, and (iii) phase variation in estimated currents.

Corresponding author:
Sai Shiva Badini,

E-mail: badinisai.eepg16@nitp.ac.in

Received: September 14, 2021

Revised: May 24, 2022

Accepted: May 25, 2022

Publication Date: September 29, 2022

DOI: 10.5152/electrica.2022.21109

Content of this journal is licensed under a Creative Commons Attribution-NonCommercial 4.0 International License.

A few methods are proposed in the literature to improve the precision and reconstruction of phase currents in all regions. Isolated current sensor tropology is adopted [28] to measure the phase currents corresponding to DC-link under zero voltage vector sampling region. As explained in [29], when the active voltage vector is short, it can be overcome by using the measurement vector insertion method. This [30] measures phase currents in the low modulation index/sector boundary region. But these methods are based on DC-link current and inverter switching states, which involve substantial complex analysis for the reconstruction of phase currents. In [31], a single-current sensor is placed on one of the motor phases, and the remaining currents are estimated from the observer design approach. But this requires phase voltages, involves complex mathematical analysis, and is dependent on machine parameters.

In this study, the rotor reference frame currents are estimated from single-current sensor, and information is presented for vector-controlled IPMSM drive. The single-current sensor is used in any one phase of the stator phases, considered phase A, and then converted to the stationary reference frame (i.e., i_α). The i_{ds}^* *and* i_{qs}^* (*d-* and *q-axes* i.e. rotor-reference frame reference currents) are used to extract the i_β^*. The *d-* and *q-axes* rotor-reference frame currents are extracted from i_α and i_β^*. The $i_{ds}^\#$ *and* $i_{qs}^\#$ currents in the rotor reference frame are closed in the current loop in the vector-controlled PMSM drive. This method is entirely independent of machine parameters. The other two-phase currents in the three phases are extracted from "*αβ*"/"*dq*" to "*abc*" transformation. However, these techniques are used for condition monitoring of sensors and drive components, to avoid sensor failure, reduce the maintenance cost, and improve the drive's reliability.

This approach predicts the remaining phase currents without any complex analysis. The IPMSM machine model is presented in Section II. The current formation technique is discussed in section III. This method is simulated and confirmed by using MATLAB/SIMULINK and presented in Section IV. Experimental results are presented in Section V, and section VI concludes the work.

II. MODELING OF INTERIOR PERMANENT MAGNET SYNCHRONOUS MOTOR

The IPMSM machine modeling is taken from [1, 32]. Equation 1 shows the stator–voltage in the rotor-reference frame (i.e., "*d-*" and "*q*"*-axes*) for IPMSM. Equation 2 shows the electrical torque developed. Equation 3 shows the electromechanical dynamics equation, where T_e and T_L are electric and load torque, respectively. Þ = derivative term $(\frac{d}{dt})$, $\omega_s = p\omega_r$, the IPMSM machine is the non-saliency type with a sinusoidal-Back–Electromotive Force (EMF) waveform. Parameters are taken from Table I.

$$\begin{pmatrix} v_{ds} \\ v_{qs} \end{pmatrix} = \begin{bmatrix} R_s + L_d Þ & -\omega_s L_q \\ \omega_s L_d & R_s + L_q Þ \end{bmatrix} \begin{pmatrix} i_{ds} \\ i_{qs} \end{pmatrix} + \begin{pmatrix} 0 \\ \omega_s \lambda_{af} \end{pmatrix} \quad (1)$$

$$T_e = \left(\frac{3}{2}\right) P\{i_{qs}\lambda_{af} + (L_d - L_q) i_{ds} i_{qs}\} \quad (2)$$

$$T_e - T_L = J\frac{d\omega_r}{dt} + B\omega_r \quad (3)$$

TABLE I. MACHINE PARAMETERS

Nominal shaft power (P_N)	3 KW
Pole pair (P)	2
Nominal speed (ω_n)	157 rad/sec
d-axis inductance (L_d)	0.0107637 H
q-axis inductance (L_q)	0.0553733 H
Mutual flux linkage between rotor and stator due to permanent magnet ($\tilde{\lambda}_{af}$)	0.553161 Wb/m^2
Stator phase winding resistance (R_s)	0.78 Ω

III. CURRENT FORMATION TECHNIQUE

The single-current sensor is placed in any motor phase terminals and is considered phase A. From the measured phase-A current, by using Clark's transformation matrix in the stationary reference frame, the *α- axis* (placed along *phase A axis*) current is calculated.

$$\begin{pmatrix} i_\alpha \\ i_\beta \end{pmatrix} = \sqrt{\frac{2}{3}} \begin{pmatrix} 1 & -0.5 & -0.5 \\ 0 & \sqrt{\frac{3}{2}} & \sqrt{\frac{3}{2}} \end{pmatrix} \begin{pmatrix} i_a \\ i_b \\ i_c \end{pmatrix} \quad (4)$$

$$i_\alpha = \sqrt{\frac{2}{3}} \left(i_a - 0.5\left(i_b + i_c\right) \right) \quad (5)$$

Under three-phase balanced current condition:

$$i_a + i_b + i_c = 0$$

$$i_b + i_c = -i_a \quad (6)$$

Substituting (6) in (5):

$$i_{\alpha s} = \sqrt{\frac{2}{3}} \left(i_a - \frac{1}{2}\left(-i_a\right) \right) \quad (7)$$

$$i_{\alpha s} = \sqrt{\frac{2}{3}} \left(\frac{3}{2}\left(i_a\right) \right) \quad (8)$$

$$i_{\alpha s} = \sqrt{\frac{3}{2}} \left(i_a\right) \quad (9)$$

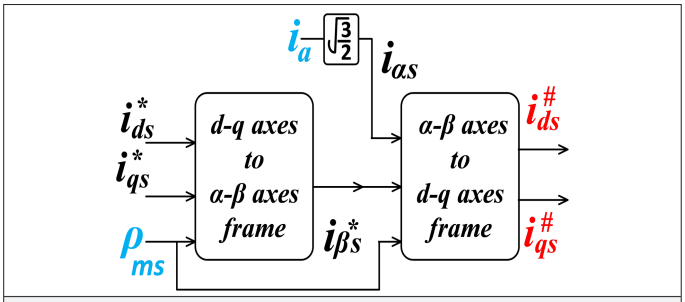

Fig. 1. Block diagram for d-q axes current formation technique.

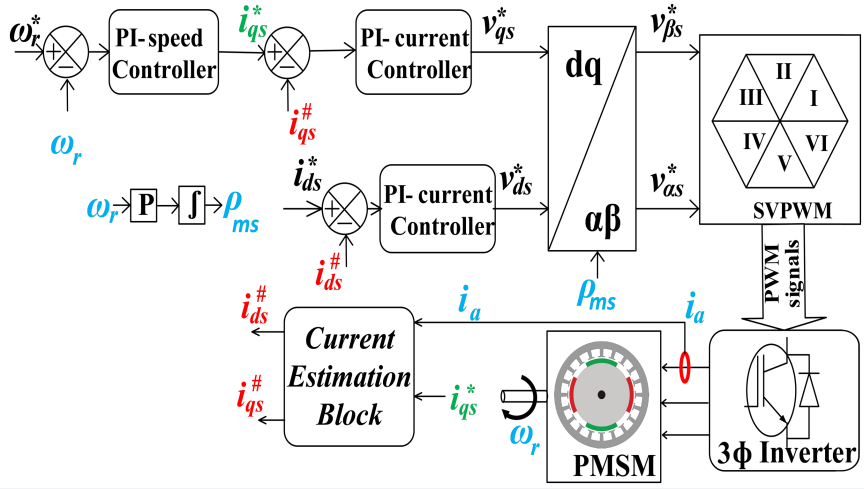

Fig. 2. Block diagram for vector-controlled IPMSM drive with a reduced current sensor. IPMSM, interior permanent magnet synchronous motor.

Using inverse park transformation from the reference currents (i.e., i_{ds}^{*} and i_{qs}^{*}) in the vector-controlled IPMSM drive:

$$\begin{pmatrix} i_{\alpha s}^{*} \\ i_{\beta s}^{*} \end{pmatrix} = \begin{pmatrix} \cos\theta_r & -\sin\theta_r \\ \sin\theta_r & \cos\theta_r \end{pmatrix} \begin{pmatrix} i_{ds}^{*} \\ i_{qs}^{*} \end{pmatrix} \tag{10}$$

For vector-controlled IPMSM drive, $i_{ds}^{*} = 0$, and i_{qs}^{*} is torque producing reference current component. Position is referred as ρ in Fig. 2 and in equations θ_r.

$$\theta_r = \int \omega_s dt = P \int \omega_r dt \tag{11}$$

$$i_{\beta s}^{*} = i_{qs}^{*} \cos\theta_r \tag{12}$$

Converting the i_{α} and i_{β}^{*} from (12) and (9) to *d*- and *q-axes* reference frame using Park transformation. The extracted currents are used to close the current loop in vector-controlled IPMSM drive.

$$\begin{pmatrix} i_{ds}^{\#} \\ i_{qs}^{\#} \end{pmatrix} = \begin{pmatrix} \cos\theta_r & \sin\theta_r \\ -\sin\theta_r & \cos\theta_r \end{pmatrix} \begin{pmatrix} i_{\alpha} \\ i_{\beta}^{*} \end{pmatrix} \tag{13}$$

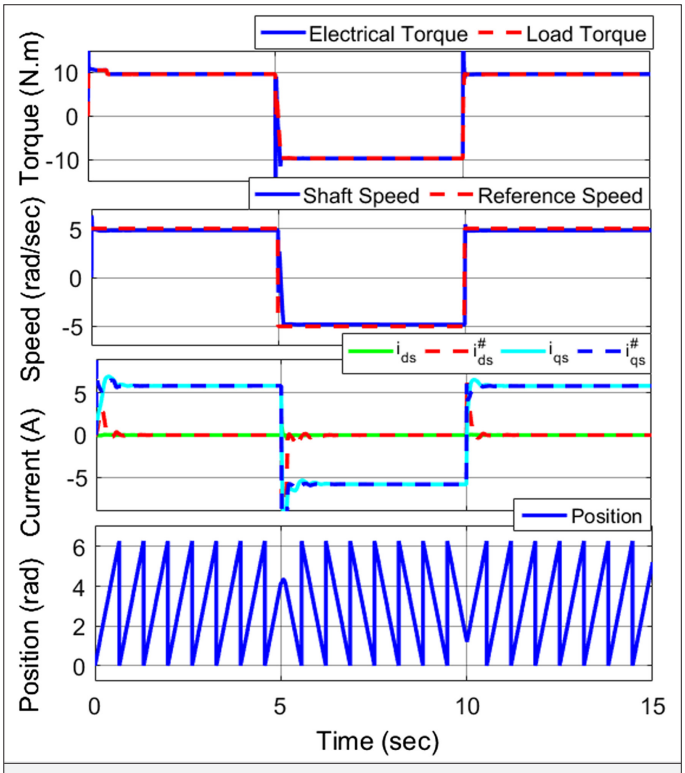

Fig. 3. Simulation results for step speed command.

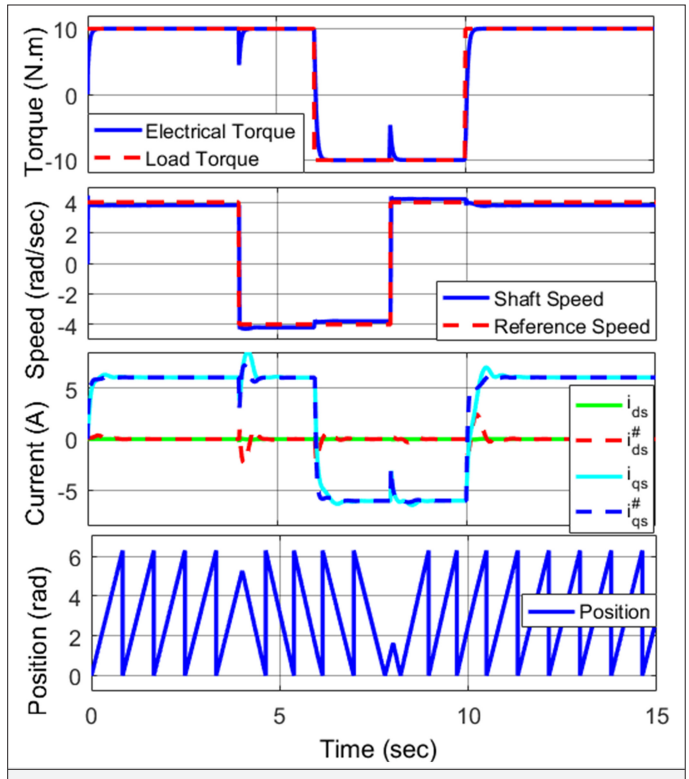

Fig. 4. Simulation results for four-quadrant operation.

$$\begin{pmatrix} i_{ds}^{\#} \\ i_{qs}^{\#} \end{pmatrix} = \begin{pmatrix} \cos\theta_r & \sin\theta_r \\ -\sin\theta_r & \cos\theta_r \end{pmatrix} \begin{pmatrix} i_\alpha \\ i_\beta^* \end{pmatrix} = \begin{pmatrix} \cos\theta_r & \sin\theta_r \\ -\sin\theta_r & \cos\theta_r \end{pmatrix} \begin{pmatrix} \sqrt{\frac{3}{2}}(i_a) \\ i_q^* \cos\theta_r \end{pmatrix} \quad (14)$$

$$i_{ds}^{\#} = \sqrt{\frac{3}{2}}(i_a)\cos\theta_r + i_q^* \sin\theta_r \cos\theta_r \quad (15)$$

$$i_{qs}^{\#} = -\sqrt{\frac{3}{2}}(i_a)\sin\theta_r + i_q^* cos^2\theta_r \quad (16)$$

Thus, under balanced conditions, we obtained 9. From the reference currents of the vector control drive, the *β-axis* current is extracted by inverse Park's transformation. The rotor position (θ_r) is obtained from actual/estimated speed from (11). The $\alpha\beta$ stator reference frame currents (i.e., i_α and i_β^* from (9) and (12)) are transformed into *d* and *q rotor-reference frame* currents by using the park's transformation. The two-phase rotor reference frame currents are estimated from a single-current sensor and are shown in (15) and (16). Fig. 1 shows the block diagram for the d-q axes current formation from a single-current information algorithm.

IV. SIMULATION RESULTS

The simulation results are presented for reduced current sensor-based vector-controlled IPMSM drive, as shown in block diagram (Fig. 2). The machine parameters are shown in Table I. The algorithm is verified for various commands, including step, ramp, low speeds, and four-quadrant operation, and are presented in this section.

A. STEP CHANGE IN REFERENCE SPEED

In Fig. 3, the reference speed is changed in a step form at $t=5$ sec and 10 sec with +5 rad/s and –5 rad/s, respectively. The load acting on the machine is DC generator type load (i.e., $K\omega_r$ Load). Here, forward and reverse motoring mode of the IPMSM drive is presented. The actual and estimated currents (*d*- and *q-axes currents*) in the rotor reference frame are presented in the same plot as i_{ds} (i.e., actual d-axes current), $i_{ds}^{\#}$ (i.e., estimated d-axes current), i_{qs} (i.e., actual q-axes current), and $i_{qs}^{\#}$ (i.e., estimated q-axes current). Shaft position information is presented in Fig. 3.

B. Four-Quadrant Operation of the Drive

The presented algorithm performance is verified for four-quadrant operation, and the simulation result is presented in Fig. 4. The reference speed is altered between +4 rad/s and –4 rad/sec at $t=4$ sec and $t=8$ sec. İnitially, machine is loaded with 10 N.m, at $t=6$ sec and $t=10$ sec, and the load is changed to –10 N.m and 10 N.m, respectively. From $t=0$ sec to $t=4$ sec and $t=10$ sec to $t=15$ sec, speed and current (i.e., i_{qs}) both are positive, showing forward motoring mode. From $t=4$ sec to 6 sec, speed is negative, but current is positive, giving reverse regeneration mode. From $t=6$ sec to $t=8$ sec, speed and current both are negative, showing reverse motoring mode of operation. From $t=8$ sec to $t=10$ sec, speed is positive, and current is negative, showing reverse regenerating mode.

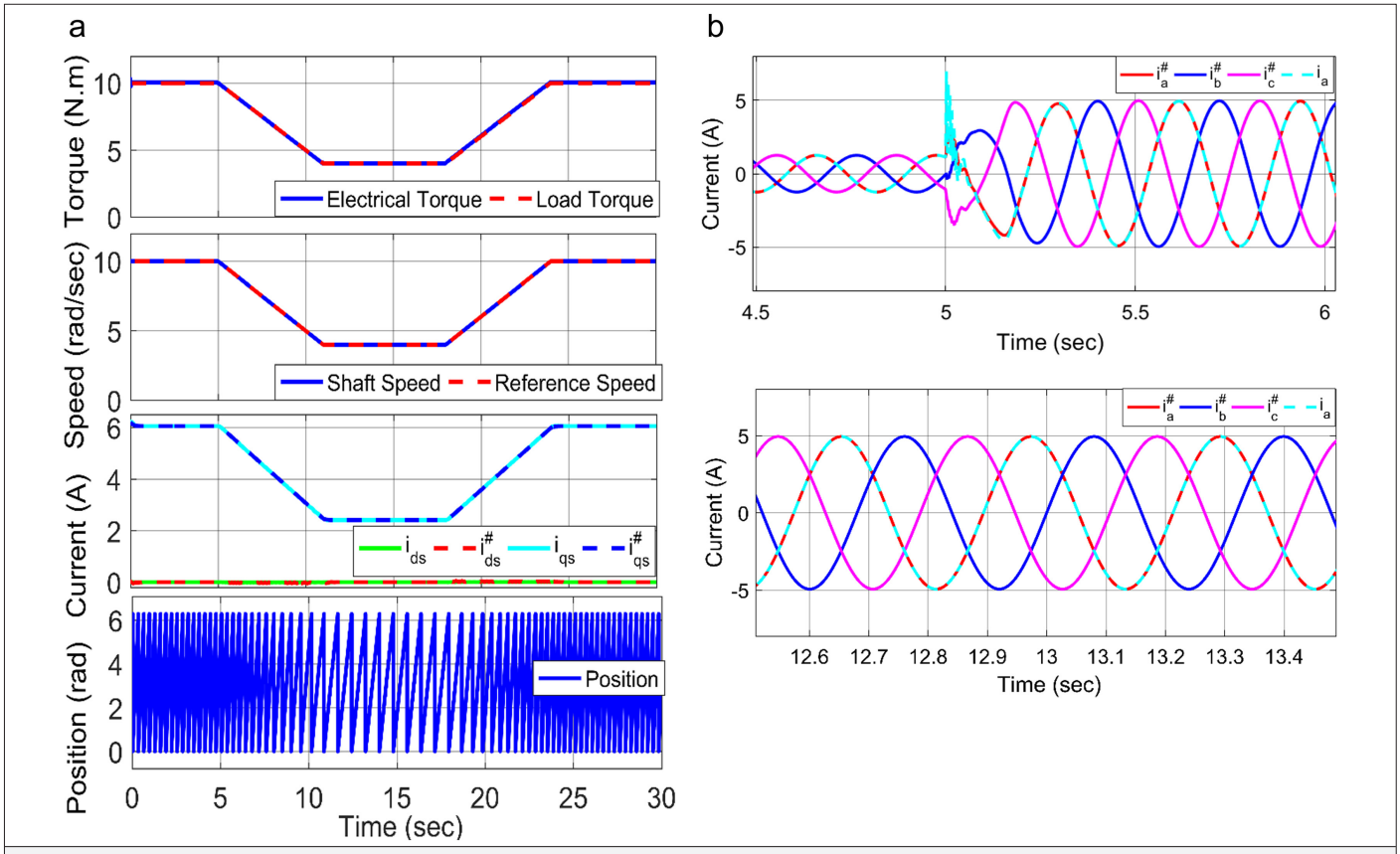

Fig. 5. Simulation results for a step change in load. (a) Load, speed, actual currents, and estimated currents and position. (b) Reconstructed three-phase currents and actual i_a.

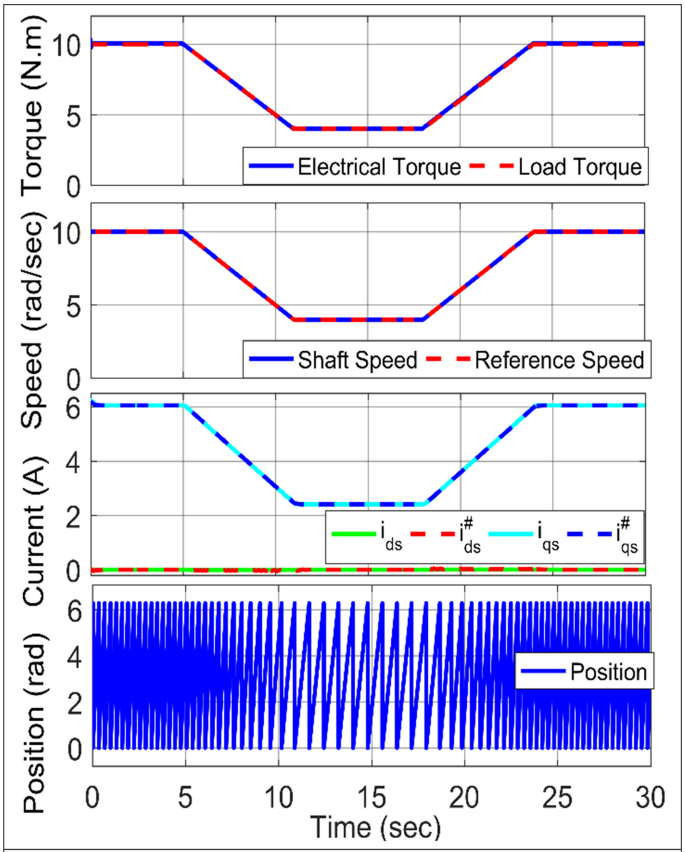

Fig. 6. Simulation results for low-speed motoring operation.

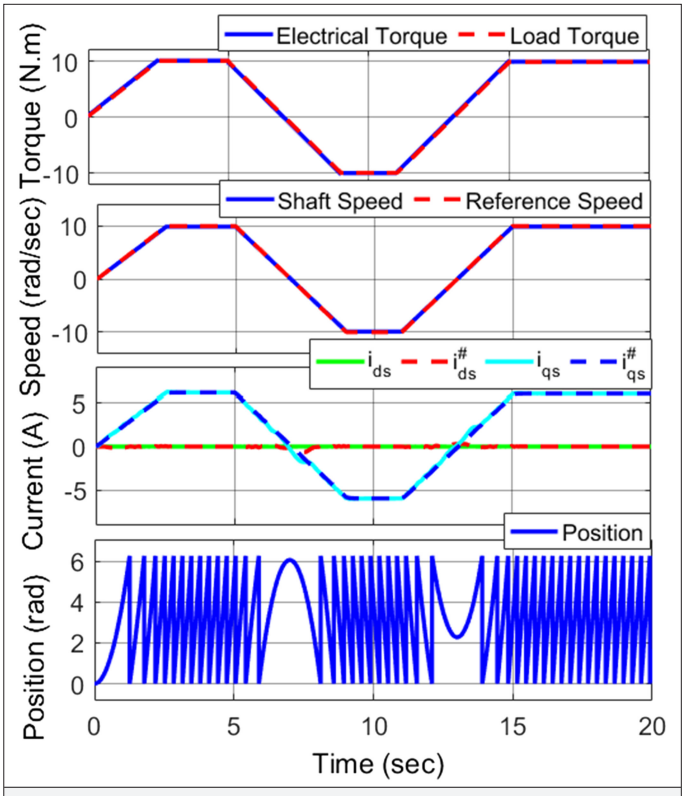

Fig. 7. Simulation results for forward and reverse motoring with slow zero crossings.

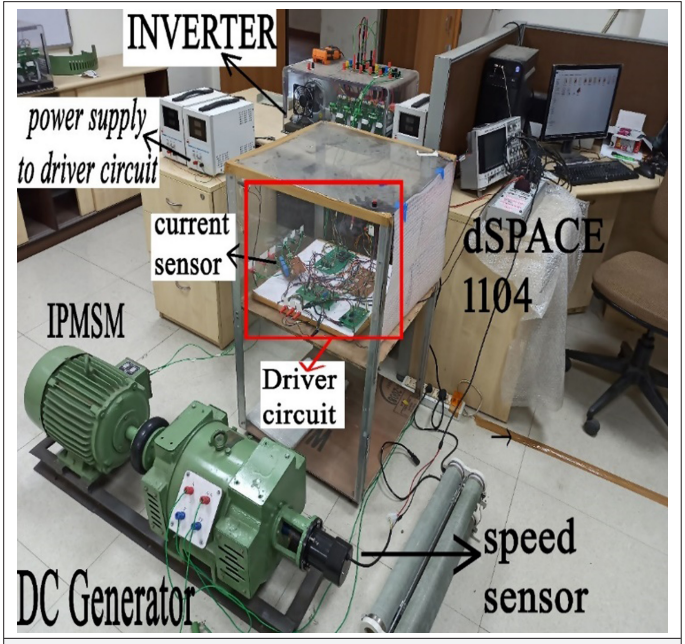

Fig. 8. Laboratory prototype-IPMSM drive. IPMSM, interior permanent magnet synchronous motor.

C. Step Change in Load

Simulation results are presented for a step change in the load for constant speed operation. The reference speed is set at 10 rad/sec, and at $t=5$ sec, the load on the machine is changed from 2.6 N.m to 10 N.m load. The estimated and actual rotor reference frame currents are plotted as shown in Fig. 5(a), and load acting on the machine, shaft speed, and position information are presented in Fig. 5(a). In Fig. 5(b), the reconstructed three-phase currents from the estimated dq-axes currents are presented with actual measure i_a current in Fig. 5(b). From Fig. 5(b), the estimated $i_a^{\#}$ phase current and i_a currents show the accuracy of the estimated current.

D. Low-Speed Operation

The simulation results are presented in Fig. 6 for low-speed forward motoring. The reference speed gradually changes from 10 rad/sec to 4 rad/sec from $t=5$ sec to $t=11$ sec and sets back to 10 rad/sec from $t=18$ sec to $t=24$ sec. The load acting on the machine is $K\omega_r$ load. The load gradually reduces and increases with speed. The shaft speed is presented along with the reference speed as shown in Fig. 6. The estimated and actual currents in the rotor reference frame are presented along with position information.

E. Response to Ramp Command and Slow Zero-Crossings

The tracking performance is verified for ramp type speed in forward and reverse motoring mode operation with slow zero crossings and is presented in Fig. 7. The reference speed is altered between +10 rad/sec to −10 rad/sec in a slow ramp command form. The constant load is acting on IPMSM, that is, DC generator type load (i.e., $K\omega_r$ load). The actual shaft speed tracks the reference speed under slow zero crossings. The actual and estimated currents in the rotor reference frame are plotted on the same graph. The simulation results show that the drive's performance with a single-current sensor performs satisfactorily under forward and reverse motoring mode.

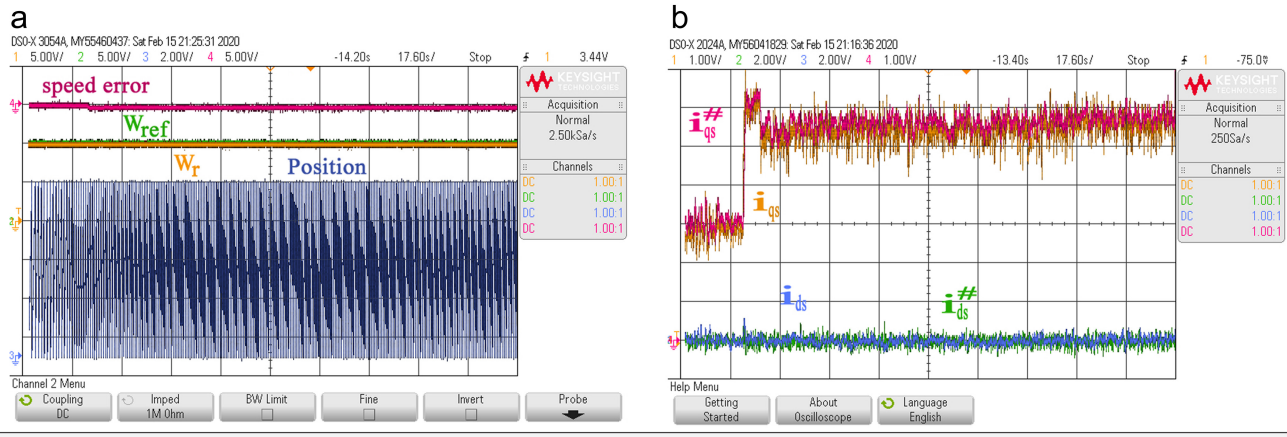

Fig. 9. Experimental results for a step change in load. (a) Shaft speed (ω_r), reference speed (ω_{ref}), speed error, and position. (b) Actual *d*- and *q-axes* stator currents (i_{ds} and i_{qs}) and estimated *d*- and *q-axes* stator currents ($i^{\#}_{ds}$ *and* $i^{\#}_{qs}$). Scale: speed: 5 rad/sec/div, current: 1A/div.

V. HARDWARE VALIDATION

The presented algorithm is verified on hardware setup developed in the laboratory using the dSPACE DS1104 IPMSM drive as shown in Fig. 8. Drive consists of dSPACE DS1104, CP1104, inverter, a Driver circuit, IPMSM, and DC generator. The d-q axes current formation technique is verified for various conditions, and some are presented for low-speed operation (forward and reverse motoring) with step load and constant load. The experimental results are presented in Figs. 9 to 11. Some experimental results are presented here for simulation results, as shown in Figs. 5 to 7. The experimental results show the shaft speed (ω_r), reference speed (ω_{ref}), actual *d* - and *q-axes stator currents* (i_{ds} and i_{qs}), and estimated *d*- and *q-axes stator currents* ($i^{\#}_{ds}$ *and* $i^{\#}_{qs}$) and with the position.

The dSPACE: real-time hardware-based technology and its input–output interface make the controller more flexible and advantageous in fields like robotics and dives. The dSPACE 1104 is more suitable for laboratory interface with a cost-effective real-time processor with I/O Interface. dSPACE is user-friendly with MATLAB/SIMULINK (real-time interface (RTI) provides Simulink blocks for I/O configuration). Using DS1104, the Simulink block is interfaced with I/O graphically, and code is generated for RTI. The model is compiled and built into the DS1104 controller board connected with PC.

The I/O signals are accessed via adapter cable from CP1104 (connector panel) to the DS1104 controller board. The CP1104 has eight ADC and eight DAC, Digital I/O, slave I/O PWM, two incremental encoders, and serial communication: RS232 and RS485. For the IPMSM drive, two ADCs are used, one for speed information and one for current sensor information. The controller board computes the control algorithm, and three-pulse width modulation (PWM) signals with 5V are generated on CP1104 (slave I/O PWM). The three PWM pulses are sent to the driver circuit board (shown in the block diagram Fig. 8). Six PWM pulses of 15V (three PWM and three inverting PWM) are generated with a delay of 2 µsec are developed and sent to drive the SEMIKRON inverter from the driver circuit board.

A) Step Change in Load

The proposed single-current sensor reduction method is verified for the step change in the load for a constant speed operation. The reference speed is set at +10 rad/sec as shown in Fig. 9. The load acting on the machine is DC generator type load (i.e., $K\omega_r$ type load). Initially, machine is loaded with 0.3 pu load. Suddenly, the load on the

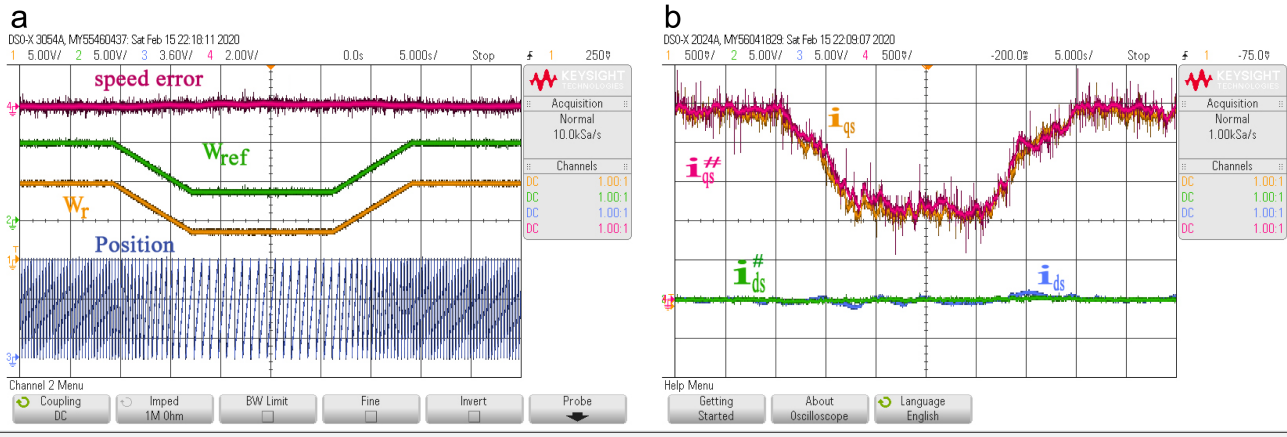

Fig. 10. Experimental results for low-speed forward motoring operation. (a) Shaft speed (ω_r), reference speed (ω_{ref}), speed error, and position. (b) Actual *d*- and *q-axes* stator currents (i_{ds} and i_{qs}) and estimated *d*- and *q-axes* stator currents ($i^{\#}_{ds}$ *and* $i^{\#}_{qs}$). Scale: speed: 5 rad/sec/div, current: 1.20 A/div.

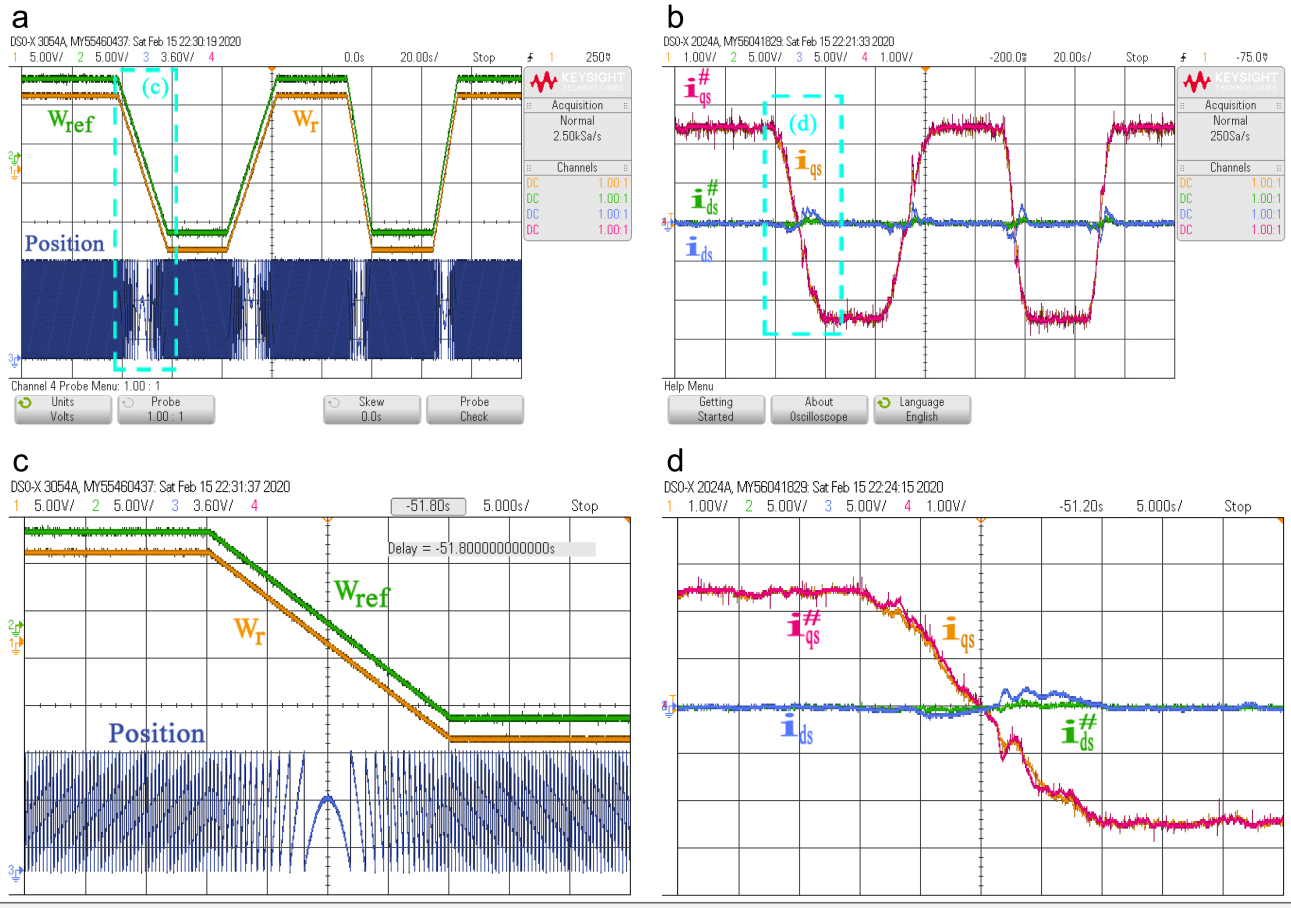

Fig. 11. Experimental results for forward and reverse motoring mode. (a) Shaft speed (ω_r), reference speed (ω_{ref}), and position. (b) Actual *d*- and *q-axes* stator currents (i_{ds} and i_{qs}) and estimated *d*- and *q-axes* stator currents ($\boldsymbol{i^{\#}_{ds}}$ ***and*** $\boldsymbol{i^{\#}_{qs}}$). Zoom plots of Fig. 11 (a) and (b), i.e., (c) speed and (d) currents, are presented. Scale: speed: 5 rad/sec/div, current: 2.5 A/div.

machine is changed to 0.6 pu by changing the resistive load on the DC generator. The reference speed and actual shaft speed are shown in Fig. 9(a). Speed error and position are also presented in Fig. 9(a). The estimated and actual currents in the rotor reference frame are presented in Fig. 9(b). The efficacy of the proposed method for vector-controlled IPMSM drive with a single-current sensor is observed as shown in Fig. 9 for a step change in load.

B) Low-Speed Operation

The proposed drive is tested for low-speed operation in forward motoring operation. The reference speed is changed from 10 rad/sec to 4 rad/sec and brought back to +10 rad/sec in a ramp form. Load acting on the machine is DC generator type load (i.e., $K\omega_r$ type load). Figure 10 shows the presented drive's hardware results in Fig. 8 with Fig. 2 configuration. Hardware results are shown for both deceleration and acceleration in low-speed motoring mode with actual and reference speed in Fig. 10(a). Speed error and position are also presented in Fig. 10(a). The estimated and actual currents in the rotor reference frame are presented in Fig. 10(b).

C) Response to Ramp Command and Slow Zero-Crossings

The proposed technique is verified for both forward motoring and reverse motoring operation. The reference speed is changed from + 10 rad/sec to –10 rad/sec in a ramp form. Load acting on the machine is DC generator type load (i.e., $K\omega_r$ type load). Both speed and current with positive magnitude show forward motoring mode, and speed and current with negative magnitude show the reverse motoring mode. Fig. 11 shows the hardware results with forward and reverse motoring modes of operation with slow zero crossing. Actual and reference speed is shown in Fig. 11(a). Speed error and position are presented in Fig. 11(a). The estimated and actual currents in the rotor reference frame are presented in Fig. 11(b). The zoom version for zero crossings is presented in Fig. 11(c) and (d). These hardware results for the proposed algorithm show satisfactory performance under various conditions.

VI. CONCLUSION

This study presents a reduced current sensor-based vector-controlled IPMSM drive. The presented d-q axes current formation algorithm is entirely independent of machine parameters and inverter switching states. This is developed based on a single-phase current sensor information and the *q-axes* reference current (i^*_{qs}) in the rotating reference frame. Three-phase currents can be reconstructed from the estimated two-phase currents. The proposed method reduces the reliability of the drive on the current sensors. The proposed method reduces a current sensor in the vector-controlled PMSM drive and can be used for monitoring the current sensor to make the drive fault-tolerant against the current sensor failure. It is also applicable to all kinds of PMSM. Permanent magnet synchronous motor

drive is developed by the proposed method, simulated in MATLAB/SIMULINK platform, and validated on the experimental model developed in the laboratory. The technique is validated by using (dSPACE 1104 controller board) IPMSM drive, and satisfactory performance is observed.

Peer-review: Externally peer-reviewed.

Author Contributions: Concept – B.S.S., V.V.; Design – B.S.S.; Supervision – V.V.; Funding – "This work was supported by the Science & Engineering Research Board (FILE NO. ECR/2016/000900), under Early Career Research Award".; Materials – B.S.S., V.V.; Data Collection and/or Processing – B.S.S., V.V.; Analysis and/or Interpretation – B.S.S.; Literature Review – B.S.S.; Writing – B.S.S.; Critical Review – V.V.

Declaration of Interests: The authors declare that they have no competing interest.

Funding: This work was supported by the Science & Engineering Research Board (file no.: ECR/2016/000900), under Early Career Research Award.

REFERENCES

1. R. Krishnan, *Permanent Magnet Synchronous and Brushless DC Motor Drives*. Boca Raton: CRC Press/Taylor & Francis, 2017.
2. B. K. Bose, "Power electronics and drives - Technology advances and trends," IEEE Int. Symp. Ind. Electron., Vol. 1, no. 8, 1999, pp. 903–908. [CrossRef]
3. P. Thamizhazhagan, and S. Sutha, "Adaptive vector control reference strategy based speed and torque control of Permanent Magnet Synchronous Motor," *Microprocess. Microsyst.*, vol. 74, p. 103007, 2020. [CrossRef]
4. B. S. Shiva, and V. Verma, "Speed and parameter estimation of vector controlled permanent magnet synchronous motor drive," in 2nd International Conference on Energy, Power and Environment: Towards Smart Technology, ICEPE 2018, Jun. 2019, pp. 1–6. [CrossRef]
5. F. Genduso, R. Miceli, C. Rando, and G. R. Galluzzo, "Back EMF sensorless-control algorithm for high-dynamic performance PMSM," *IEEE Trans. Ind. Electron.*, vol. 57, no. 6, pp. 2092–2100, Jun. 2010. [CrossRef]
6. H. M. Kojabadi, and M. Ghribi, "MRAS-based adaptive speed estimator in PMSM drives," *Int. Work Adv. Motion Control. AMC*, vol. 2006, no. 1, pp. 569–572, 2006. [CrossRef]
7. Y. Inoue, Y. Kawaguchi, S. Morimoto, and M. Sanada, "Performance improvement of sensorless IPMSM drives in a low-speed region using online parameter identification," *IEEE Trans. Ind. Appl.*, vol. 47, no. 2, pp. 798–804, Mar. 2011. [CrossRef]
8. P. Kshirsagar, and R. Krishnan, "Sensorless position control of PMSM operating at low switching frequency for high efficiency climate control systems," *IEEE Int.* Electr. Mach. Drives Conf. IEMDC, Vol. 2017, no. Aug., 2017. [CrossRef]
9. D. Xu, S. Zhang, and J. Liu, "Very-low speed control of PMSM based on EKF estimation with closed loop optimized parameters," *ISA Trans.*, vol. 52, no. 6, pp. 835–843, 2013. [CrossRef]
10. S. Singh, and A. N. Tiwari, "Various techniques of sensorless speed control of PMSM: A review," 2017 *Second International Conference on Electrical, Computer and Communication Technologies ICECCT*, 2017, pp. 1–6. [CrossRef]
11. Y. S. Kim, Y. K. Choi, and J. H. Lee, "Speed-sensorless vector control for permanent-magnet synchronous motors based on instantaneous reactive power in the wide-speed region," *IEE Proc. Electr. Power Appl.*, vol. 152, no. 5, pp. 1343–1349, 2005. [CrossRef]
12. J. M. Liu, and Z. Q. Zhu, "Improved sensorless control of permanent-magnet synchronous machine based on third-harmonic back EMF," *IEEE Trans. Ind. Appl.*, vol. 50, no. 3, pp. 1861–1870, 2014. [CrossRef]
13. Hongryel Kim, Jubum Son, and Jangmyung Lee, "A high-speed sliding-mode observer for the sensorless speed control of a PMSM," *IEEE Trans. Ind. Electron.*, vol. 58, no. 9, pp. 4069–4077, Sep. 2011. [CrossRef]
14. D. W. Chung, and S. K. Sul, "Analysis and compensation of current measurement error in vector-controlled AC motor drives," *IEEE Trans. Ind. Appl.*, vol. 34, no. 2, pp. 340–345, 1998. [CrossRef]
15. F. Blaabjerg, J. K. Pedersen, U. Jaeger, and P. Thoegersen, "Single current sensor technique in the DC-link of three-phase PWM-VS inverters a review and the ultimate solution," in Conference Record - IAS Annual Meeting, IEEE Industry Applications Society, 1996, vol. 2, pp. 1192–1202. [CrossRef]
16. B. Saritha, and P. A. Janakiraman, "Sinusoidal three-phase current reconstruction and control using a DC-link current sensor and a curve-fittins observer," *IEEE Trans. Ind. Electron.*, vol. 54, no. 5, pp. 2657–2664, 2007. [CrossRef]
17. D. C. Lee, and D. S. Lim, "AC voltage and current sensorless control of three-phase PWM rectifiers," *IEEE Annual Power Electronics Specialists Conference*, in PESC Record, Vol. 2, 2000, pp. 588–593. [CrossRef]
18. B. Metidji, N. Taib, L. Baghli, T. Rekioua, and S. Bacha, "Novel single current sensor topology for Venturini controlled direct matrix converters," *IEEE Trans. Power Electron.*, vol. 28, no. 7, pp. 3509–3516, 2013. [CrossRef]
19. S. Li, B. Bai, and D. Chen, "Vector control of permanent magnet synchronous motor by using single current sensor," in *ICPE*, 2019 - E. Asia, 2019 - 10th International Conference on Power Electronics - ECCE Asia, pp. 2556–2561. Available: https://ieeexplore.ieee.org/document/8797255.
20. V. Verma, C. Chakraborty, S. Maiti, and Y. Hori, "Speed Sensorless vector controlled induction motor drive using single current sensor," *IEEE Trans. Energy Convers.*, vol. 28, no. 4, pp. 938–950, 2013. [CrossRef]
21. J. T. Boys, "Novel current sensor for PWM AC drives," *IEE Proc. B Electr. Power Appl. UK*, vol. 135, no. 1, pp. 27–32, 1988. [CrossRef]
22. T. C. Green, and B. W. Williams, "Derivation of motor line-current waveforms from the DC-link current of an inverter," *IEE Proc. B Electr. Power Appl. UK*, vol. 136, no. 4, pp. 196–204, 1989. [CrossRef]
23. J. Zhao, S. Nalakath, and A. Emadi, "A high frequency injection technique with modified current reconstruction for low-speed sensorless control of IPMSMs with a single dc-link current sensor," *IEEE Access*, vol. 7, pp. 136137–136147, 2019. [CrossRef]
24. Q. Tang, A. Shen, W. Li, P. Luo, M. Chen, and X. He, "Multiple-positions-coupled sampling method for PMSM three-phase current reconstruction with a single current sensor," *IEEE Trans. Power Electron.*, vol. 35, no. 1, pp. 699–708, Jan. 2020. [CrossRef]
25. L. Zhu *et al.*, "Phase current reconstruction error suppression method for single DC-link shunt PMSM drives at low-speed region," *IEEE Trans. Power Electron.*, vol. 37, no. 6, 7067–7081, 2021. [CrossRef]
26. G. Wang *et al.*, "Current Reconstruction Considering Time-Sharing Sampling Errors change throughout the running heads," *IEEE Trans. Power Electron.*, vol. 36, no. 5, pp. 5760–5770, 2021. [CrossRef]
27. M. Aktaş, and B. Çavuş, "Current reconstruction for PMSM drives using a DC-link single current sensor," *Electrica*, vol. 22, no. 1, pp. 101–108, 2022. [CrossRef]
28. Y. Xu, H. Yan, J. Zou, B. Wang, and Y. Li, "Zero voltage vector sampling method for PMSM three-phase current reconstruction using single current sensor," *IEEE Trans. Power Electron.*, vol. 32, no. 5, pp. 3797–3807, 2017. [CrossRef]
29. J. I. Ha, "Voltage injection method for three-phase current reconstruction in PWM inverters using a single sensor," *IEEE Trans. Power Electron.*, vol. 24, no. 3, pp. 767–775, 2009. [CrossRef]
30. Yikun Gu, Fenglei Ni, Dapeng Yang, and Hong Liu, "Switching-state phase shift method for three-phase-current reconstruction with a single dc-link current sensor," *IEEE Trans. Ind. Electron.*, vol. 58, no. 11, pp. 5186–5194, 2011. [CrossRef]
31. Q. Teng, H. Cui, J. Duan, J. Zhu, Y. Guo, and G. Lei, "Extended state observer-based vector control for PMSM drive system with single phase current sensor," in 20th International Conference on Electrical Machines and Systems, ICEMS 2017, 2017. [CrossRef]
32. S. S. Badini, and V. Verma, "MRAS-based speed and parameter estimation for a vector-controlled PMSM drive," *Electrica*, vol. 20, no. 1, pp. 28–40, 2020. [CrossRef]